A new statistically based autoconversion rate parameterization for use in large-scale models

Junhua Zhang and Ulrike Lohmann
Department of Physics and Atmospheric Science, Dalhousie University, Halifax, Nova Scotia, Canada

Bing Lin
NASA Langley Research Center, Hampton, Virginia, USA

Received 12 November 2001; revised 16 April 2002; accepted 13 June 2002; published 19 December 2002.

[1] The autoconversion rate is a key process for the formation of precipitation in warm clouds. In climate models, physical processes such as autoconversion rate, which are calculated from grid mean values, are biased, because they do not take subgrid variability into account. Recently, statistical cloud schemes have been introduced in large-scale models to account for partially cloud-covered grid boxes. However, these schemes do not include the in-cloud variability in their parameterizations. In this paper, a new statistically based autoconversion rate considering the in-cloud variability is introduced and tested in three cases using the Canadian Single Column Model (SCM) of the global climate model. The results show that the new autoconversion rate improves the model simulation, especially in terms of liquid water path in all three case studies. *INDEX TERMS:* 0320 Atmospheric Composition and Structure: Cloud physics and chemistry; 3337 Meteorology and Atmospheric Dynamics: Numerical modeling and data assimilation; 3354 Meteorology and Atmospheric Dynamics: Precipitation (1854); *KEYWORDS:* autoconversion rate, statistical cloud scheme, subgrid-scale variability, cloud modeling, ARM, SHEBA

Citation: Zhang, J., U. Lohmann, and B. Lin, A new statistically based autoconversion rate parameterization for use in large-scale models, *J. Geophys. Res.*, *107*(D24), 4750, doi:10.1029/2001JD001484, 2002.

1. Introduction

[2] About 60% of the Earth's surface is covered by clouds. They are an important regulator of the Earth's radiation budget. Earth Radiation Budget Experiment (ERBE) measurements shows that clouds cool the Earth–atmosphere system by 48 W m^{-2} in the solar spectrum and warm it by 30 W m^{-2} in the infrared [*Collins et al.*, 1994]. The lack of understanding of clouds remains one of the largest uncertainties in climate modeling and prediction [*Houghton et al.*, 1996].

[3] One of the key physical processes that determine cloud liquid water path, precipitation and cloud cover is the autoconversion of cloud droplets to form drizzle-size drops. There are two approaches to parameterize autoconversion in GCMs (General Circulation Models). One is a threshold-dependent parameterization [*Boucher et al.*, 1995; *Rotstayn*, 1997], where autoconversion is suppressed when the volume-mean cloud-droplet radius is below a given threshold. Another approach is a continuous parameterization derived from the stochastic collection equation [*Beheng*, 1994; *Lohmann and Roeckner*, 1996]. Both of them depend nonlinearly on the cloud water content. In a large-scale model like a GCM, the unresolved subgrid variance provides a challenge for nonlinear process. *Pincus and Klein* [2000] demonstrated that because of the nonlinear dependence of the autoconversion rate on the cloud condensate concentration, the process rates computed using the grid mean value are underestimated by as much as a factor of 2.

[4] For partial cloudiness, a probability distribution function (PDF) based parameterization, which was originally used by *Sommeria and Deardorff* [1977] in a high-resolution cloud model, was introduced into large-scale models [e.g., *Smith*, 1990; *Richard and Royer*, 1993; *Xu and Randall*, 1996; *Lohmann et al.*, 1999; *Abdella and McFarlane*, 2001]. In this scheme, the total water mixing ratio (sum of water vapor and condensed water), is assumed to follow a certain statistical distribution. This PDF based method consistently prognoses the subgrid cloud fraction and total cloud water in the cloudy part of the grid box. However, it still does not consider the variability of cloud water within the cloud. For a highly nonlinear process such as the autoconversion rate, this neglect can lead to an unreasonable tuning in the parameterization. For example, in the continuous autoconversion parameterization used by *Lohmann and Roeckner* [1996] in the ECHAM GCM, the autoconversion rate is arbitrarily increased by a factor of 15 to achieve a satisfactory simulation. In the threshold-dependent autoconversion parameterization, the threshold cloud droplet radius is also set to an unrealistic small value (4.5 μm–7.5 μm) in large-scale models [*Boucher et al.*, 1995; *Rotstayn*, 1998; *Wilson and Ballard*, 1999].

[5] *Rotstayn* [2000] applied the subgrid total water distribution from the model's condensation scheme in a threshold-

0148-0227/02/2001JD001484$09.00

dependent autoconversion parameterization and increased the threshold cloud droplet radius from 7.5 μm to a more reasonable value of 9.3 μm, while maintaining the global mean liquid water path at about the same value. In his method, the mean in-cloud value of liquid water content does not need to exceed the threshold for autoconversion to occur, as long as the mean value in some part of the cloudy area exceeds the threshold. The autoconversion rate, however, is still calculated using the mean value of liquid water content in that part of the cloudy area.

[6] In this paper, we will introduce a new statistically based continuous autoconversion parameterization considering in-cloud variability of liquid water content, and verify it using the Canadian Single Column Model (SCM). The model is described in section 2. Section 3 explains the derivation of the new parameterization. The validation of this new parameterization is tested in three case studies (section 4). Two of the cases are two intensive observation periods (IOP) of Atmospheric Radiation Measurement (ARM) program in the Southern Great Plains (SGP), Oklahoma (centered at 97.49°W, 36.61°N), one from 15 September to 6 October 1997, another from 1 March to 22 March 2000. The third one is the Surface Heat Budget of the Arctic Ocean (SHEBA) experiment. The measurements of this experiment were obtained on board the SHEBA ship that was set adrift through the Arctic sea ice from November 1997 to September 1998 (the position of the ship was within 144°–169°W, 74°–81°N). Summary and conclusions are then given in section 5.

2. Model Description

[7] One way of validating physical processes in a general circulation model (GCM) is to use a model that includes the processes that are represented in a single-column of a GCM. Such a SCM is in dynamical isolation from the rest of the GCM and can be forced every time step by advection obtained from observational data or operational analysis [*Randall et al.*, l996] or being nudged toward them. In this approach the differences between the SCM simulations and observations are attributable to the effects of physical parameterizations. "Nudging" means that the prognostic variables such as temperature and wind are "relaxed" toward the observed state. The difficulty is to find a nudging coefficient that is large enough to force the model close enough toward the observations but small enough to allow the model to develop its own physical processes. We applied this approach successfully during the North Atlantic Regional Experiment (NARE) case study [*Lohmann et al.*, 1999], and to the First ISCPP Regional Experiment–Arctic Cloud Characterization Experiment (FIRE.ACE) [*Lohmann et al.*, 2001]. Here we apply it to test the new autoconversion parameterization. The nudging time step we chose for our SCM simulation is dependent on wind speed $\left(\tau = \frac{\Delta X}{\sqrt{U^2+V^2}}\right)$ [see *Ghan et al.*, 2000]. It adjusts temperature and specific humidity from the SCM toward the forcing data. Here ΔX refers to the size of the grid box. The global climate model grid would be a 3.75° × 3.75° grid. This corresponds to a distance of 100 km in longitude at 76° N and 332 km at 37° N, and to a distance in latitude of 416 km. Therefore we use ΔX to be 250 km for the SHEBA case and 375km for the ARM case studies.

[8] The SCM we used is the Canadian Centre for Climate Modeling and Analysis (CCCMA) SCM. The prognostic variables of the CCCMA SCM are temperature, water vapor and the number concentration and mass mixing ratio of cloud liquid water and cloud ice [*Lohmann et al*, 1999]. The model equations are solved on 29 vertical levels with a top at 12 hPa using a time step of 15 min.

[9] The turbulence scheme contains a prognostic equation for the turbulent kinetic energy (TKE) [*Abdella and McFarlane*, 1997]. Other second-order moments, including countergradient and nonlocal effects, are determined diagnostically through a parameterization of the third-order moments which is based on a convective mass-flux argument. Cumulus clouds are represented by a bulk model, including the effects of entrainment and detrainment on the updraft and downdraft convective mass fluxes [*Zhang and McFarlane*, 1995]. The radiation code is based on a two-stream solution of the radiative transfer equation with six spectral intervals in the terrestrial infrared spectrum [*Morcrette*, 1991] and two in the solar part of the spectrum [*Fouquart and Bonnel*, 1980]. Gaseous absorption due to water vapor, CO_2, O_3, CH_4, N_2O, and CFCs is included, as well as scattering and absorption due to prescribed aerosols and model-generated clouds.

[10] The cloud scheme used in this study is described in detail by *Lohmann et al.* [1999]. Parameterized microphysical processes are condensational growth of cloud droplets, depositional growth of ice crystals, homogeneous and heterogeneous freezing of cloud droplets, autoconversion of cloud droplets, aggregation of ice crystals, accretion of cloud ice and cloud droplets by snow, of cloud droplets by rain, evaporation of cloud liquid water and rain, sublimation of cloud ice and snow, and melting of cloud ice and snow. The precipitation formation rates for mixed and ice clouds are adopted from the formulations used in the mesoscale model GESIMA [*Levkov et al.*, 1992], while those for warm clouds are derived from the stochastical collection equation [*Beheng*, 1994]. Fractional cloud cover and liquid water content are diagnostically calculated by a statistical cloud scheme following the ideas of *Sommeria and Deardorff* [1977].

[11] In a statistical cloud scheme, the evolution of condensed water in stratiform clouds is described in terms of total water q_t (sum of water vapor and condensed water) and the condensed water potential temperature because both quantities are conserved variables when condensation occurs in the absence of precipitation. The large-scale mean values of these quantities are prognostic fields in the model while the unresolved components are assumed to be distributed in a statistical manner around these mean values.

[12] Following the previous practices [e.g., *Sommeria and Deardorff*, 1977; *Lohmann et al.*, 1999], we define a single variable S in terms of the difference between the total water within the grid volume and that which would exist if the air were just saturated:

$$s = a_l(q_t - q_{sl}) \tag{1}$$

where q_{sl} is the saturation vapor mixing ratio with respect to the liquid water temperature T_l. Because of the fluctuation in the grid box, its local deviation from the mean is:

$$s' = a_l\left(q'_t - \alpha_l T'_l\right) \tag{2}$$

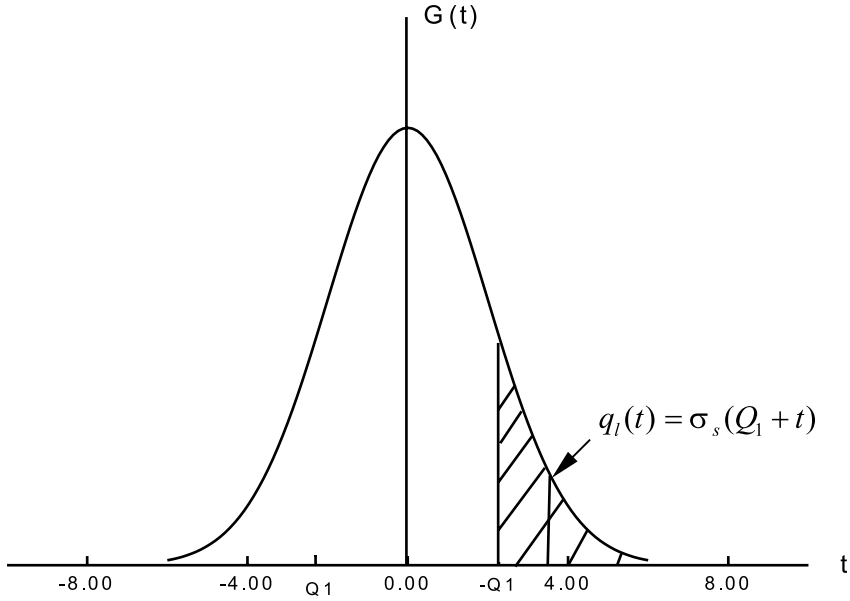

Figure 1. Gaussian distribution function G(t) used by statistical cloud scheme. The cloudy area is hatched.

where the coefficients a_l and α_l are given as

$$\alpha_l = \frac{\partial q_{sl}}{\partial T} \tag{3}$$

$$a_l = \left[1 + \frac{L}{c_p}\alpha_l\right]^{-1} \tag{4}$$

L is the latent heat of vaporization and c_p is the specific heat of dry air at constant pressure, and a_l accounts for latent heating.

[13] The grid-box mean of s' is zero since $\overline{q_t'}$ and $\overline{T_l'}$ are zero. The standard deviation of s' (σ_s) is given by:

$$\sigma_s = a_l\sqrt{\overline{q_t'^2} + \alpha_l^2\overline{T_l'^2} - 2\alpha_l\overline{q_t'T_l'}} \tag{5}$$

We then introduce variables Q_1 and t that are s and s' normalized by σ_s:

$$Q_1 = \frac{s}{\sigma_s} = a_1(q_t - q_{sl})/\sigma_s \tag{6}$$

$$t = \frac{s'}{\sigma_s} \tag{7}$$

Then the local cloud water content is given as

$$q_l(t) = \begin{cases} 0 & t \le -Q_1 \\ \sigma_s(Q_1 + t) & t > -Q_1 \end{cases} \tag{8}$$

[14] Given a distribution function G for the normalized variable t, the cloud fraction is the fraction of the grid box where the cloud water content is greater than zero, as illustrated in Figure 1, the cloudy area is shaded in this figure, and is given by:

$$b = \int_{-Q_1}^{\infty} G(t)dt \tag{9}$$

The ensemble mean cloud water content can be expressed as

$$q_l = \sigma_s\int_{-Q_1}^{\infty}(Q_1 + t)G(t)dt \tag{10}$$

Several different distribution functions including symmetric and skewed have been used in different studies. Here we assume a Gaussian distribution function for G as shown in Figure 1.

$$G(t) = \frac{1}{\sqrt{2\pi}}\exp\left(-t^2/2\right) \tag{11}$$

Cloud fraction and total cloud water content are then given by

$$b = \frac{1}{2}\left(1 + erf\frac{Q_1}{\sqrt{2}}\right), q_l = \sigma_s\left(bQ_1 + \frac{e^{-Q_1^2/2}}{\sqrt{2\pi}}\right) \tag{12}$$

[15] For small-scale fluctuation, the standard deviation σ_s can be determined by a higher order turbulence closure scheme. However, in a large-scale model like a GCM, the subgrid-scale fluctuations not only include small-scale turbulence, but also include mesoscale effects. Therefore, we use an expression for σ_s derived by *Smith* [1990] for a triangle distribution function.

$$\sigma_s = \left\{(1 - RHc)/\sqrt{6}\right\}a_l q_{sl}(T_l, p) \tag{13}$$

Where RHc is a threshold relative humidity. It is set to 0.85 for the ARM cases following *Smith* [1990]. For the SHEBA case, too little cloud coverage is simulated with RHc = 0.85, so that we reduced RHc to 0.70 to improve the agreement of the simulated cloud cover with observations. Similar conclusions that parameterizations for midlatitude clouds

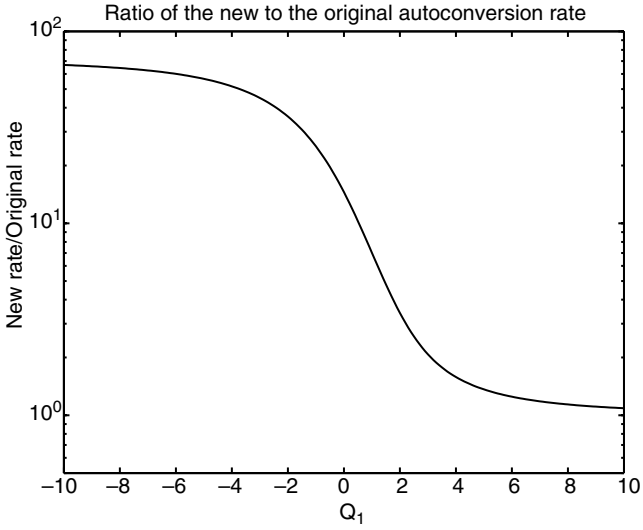

Figure 2. Ratio of the new to the original autoconversion rate as function of Q_1.

in terms of ice nucleation cannot be applied without adjustment to Arctic clouds were reached by *Jiang et al.* [2000] who studied mixed-phase Arctic stratus.

3. Treatment of Autoconversion Parameterization

3.1. Original Autoconversion Rate

[16] In our SCM, the original autoconversion rate Q_{aut} [kg kg^{-1} s^{-1}] is derived from the stochastic collection equation as given by *Beheng* [1994] (in SI units)

$$Q_{aut} = \left(6 \cdot 10^{28} n^{-1.7} \left(10^{-6} N_l\right)^{-3.3} \left(10^{-3} \rho q_{cl}\right)^{4.7}\right)/\rho \qquad (14)$$

where n(= 10) is the width parameter of the initial cloud droplet spectrum; N_t is the cloud droplet concentration; ρ is the air density and q_{cl} is the cloud water mixing ratio in the cloudy part of the grid box

$$q_{cl} = q_l/b \qquad (15)$$

where q_l and b are given by (12).

3.2. New Autoconversion Rate

[17] The autoconversion rate obtained in (14) is calculated from the mean in-cloud water mixing ratio in the cloudy area of the grid box. It does not consider the variability of liquid water in the cloudy part. To include this variability in the new parameterization, we integrate the autoconversion rate according to the distribution of liquid water in the cloudy part as described below.

[18] For simplicity, we rewrite (14) as

$$Q_{aut} = \alpha q_{cl}^{4.7} \qquad (16)$$

where α includes all other parameters that determine the autoconversion rate except q_{cl}.

[19] In the grid box, $q_l(t)$ is given by (8), so that when $t > -Q_1$, the autoconversion rate in different parts of the cloud can be expressed as:

$$Q_{aut}(t) = \alpha[\sigma_s(Q_1 + t)]^{4.7} \qquad t > -Q_1 \qquad (17)$$

Since the probability for t with values t to $t + dt$ is $G(t)dt$, that the probability for Q_{aut} with values from $Q_{aut}(t)$ to $Q_{aut}(t + dt)$ is also $G(t)dt$, thus the ensemble mean autoconversion rate is given by

$$Q_{aut}(t) = \alpha\sigma_s^{4.7} \int_{-Q_1}^{\infty} (Q_1 + t)^{4.7} G(t)dt \qquad (18)$$

For a Gaussian distribution function, (18) gives

$$Q_{aut} = \frac{1}{\sqrt{2\pi}} \alpha\sigma_s^{4.7} \int_{-Q_1}^{\infty} (Q_1 + t)^{4.7} \exp\left(-t^2/2\right)dt \qquad (19)$$

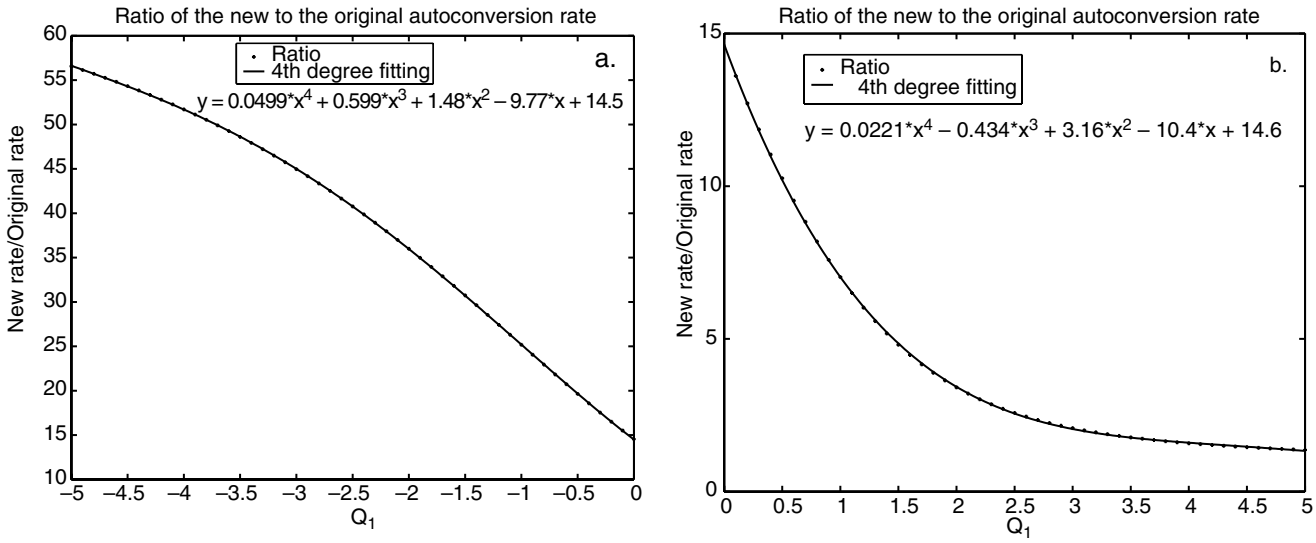

Figure 3. Polynomial fit of the ratio of the new to the original autoconversion rate. a) for negative Q_1, b) for positive Q_1.

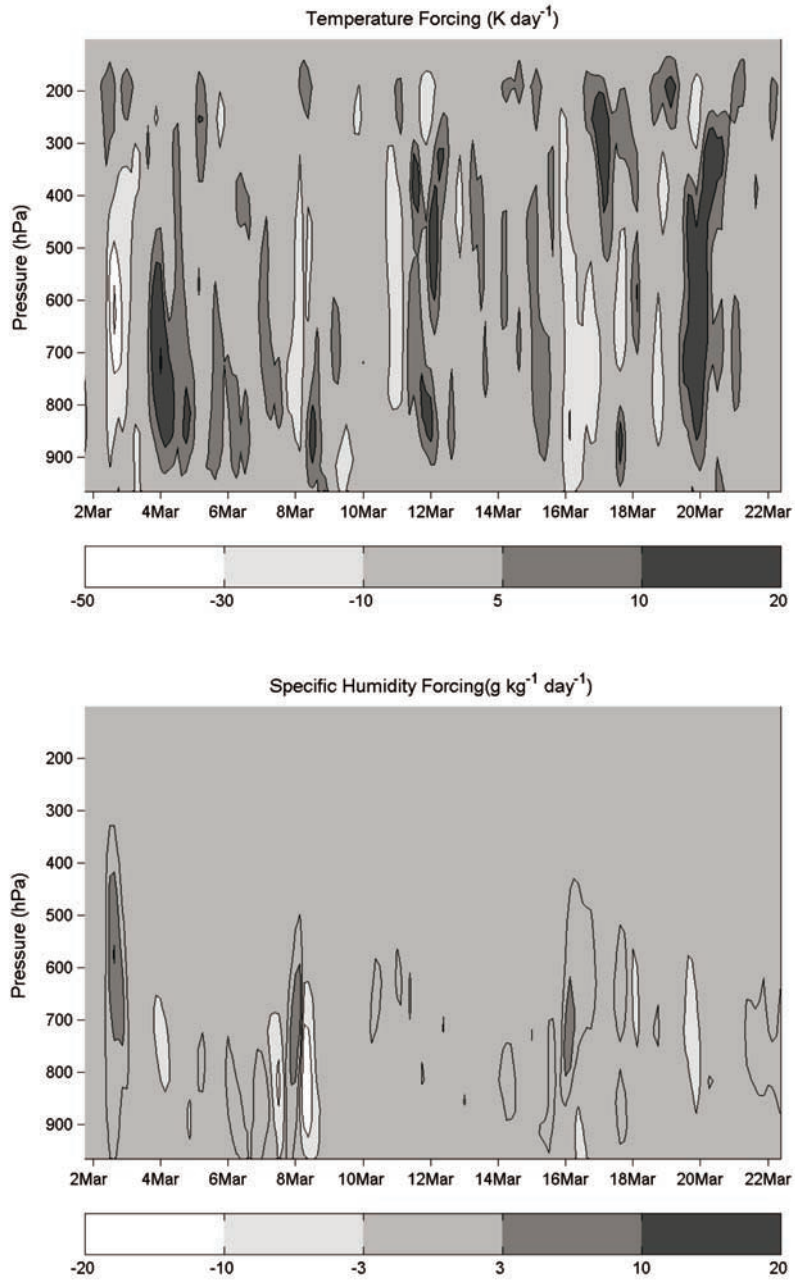

Figure 4. Hovmőller diagram of the temperature forcing (K day^{-1}) and specific humidity forcing (g kg^{-1} day^{-1}) during the period 1 March–22 March 2000.

with that the "Equivalent Autoconversion Rate" in the cloud is defined by

$$Q_{eqaut} = \frac{Q_{aut}}{b} \tag{20}$$

4. Results and Discussion

[20] Equation (19) can not be integrated analytically. Therefore we obtain the new autoconversion rate by applying a polynomial fit to the numerical integration of (19) for different values of Q_1.

[21] Figure 2 is the ratio of the new to the original autoconversion rate over a large range of Q_1 ($-10 \leq Q_1 \leq 10$). The new autoconversion rate is larger than the original one, especially for the negative values of Q_1. The largest gradient in the ratio occurs for Q_1 around 0. For $5 \leq Q_1$ and $Q_1 \leq -5$, the ratio can be deemed constant, 1.3 and 60 respectively. Figures 3a and 3b show the polynomial fits for negative ($-5 \leq Q_1 \leq 0$) and positive ($0 \leq Q_1 \leq 5$) value of Q_1,

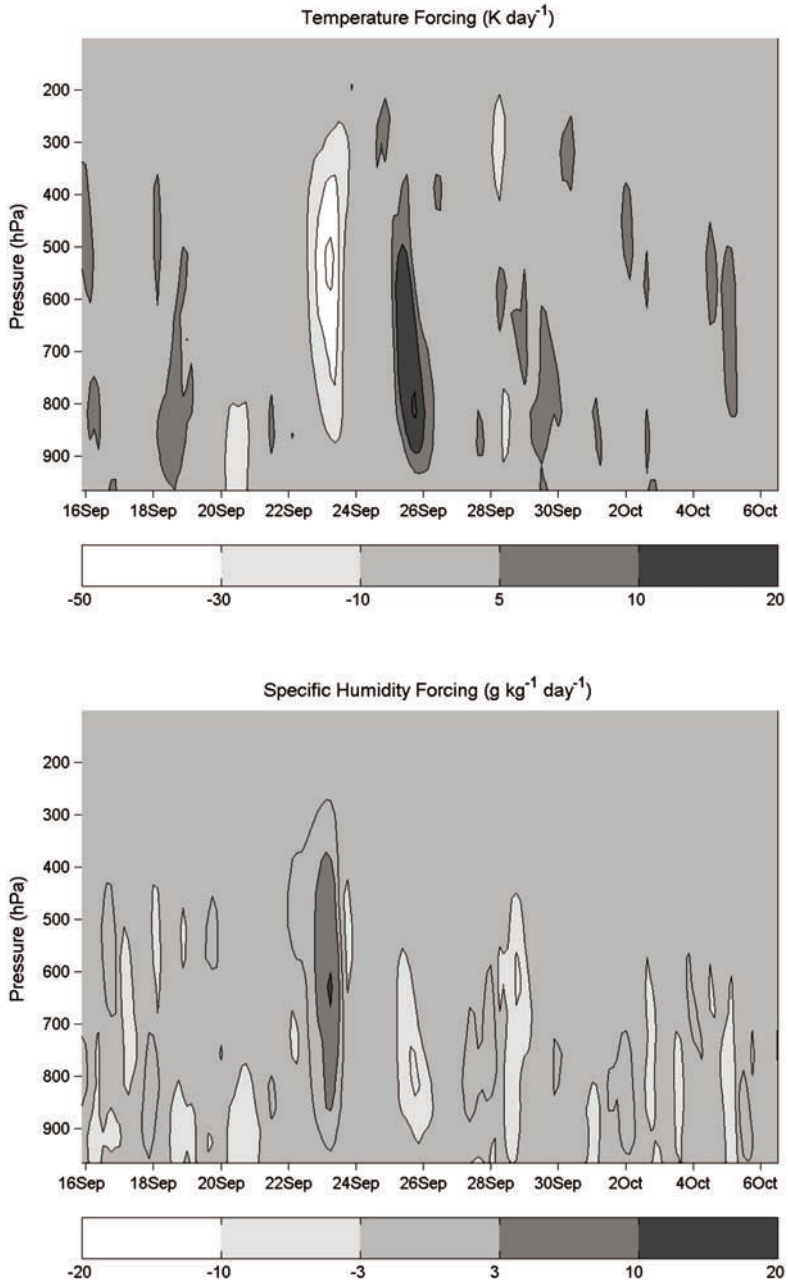

Figure 5. Hovmőller diagram of the temperature forcing (K day^{-1}) and specific humidity forcing (g kg^{-1} day^{-1}) during the period 15 September to 6 October 1997.

respectively. A 4th degree polynomial fit is needed to get a good result.

4.1. Simulation of ARM Cases

[22] The Atmospheric Radiation Measurement Program (ARM) is the largest global change research program supported by the U.S. Department of Energy (DOE). It focuses on obtaining field measurements and developing models to better understand the processes that control solar and thermal infrared radiative transfer in the atmosphere (especially in clouds) and at the Earth's surface [http://dev.www.arm.gov/docs/index.html]. In our two case studies, the SCM is driven every 3 hours by observed vertical profiles of temperature, specific humidity, three dimensional wind velocities, temperature and specific humidity tendencies which are specially prepared for SCM simulations [*Zhang and Lin*, 1997; *Zhang et al.*, 2001].

[23] A more detailed description of the ARM SGP site, data measurement and the methods for running the SCM simulations are discussed by *Ghan et al.* [2000]. Figures 4 and 5 show the temperature and specific humidity tendencies as a function of pressure and time for the spring and the fall case, respectively. In the spring IOP, there were several events with strong cold air advection (larger than 30 K

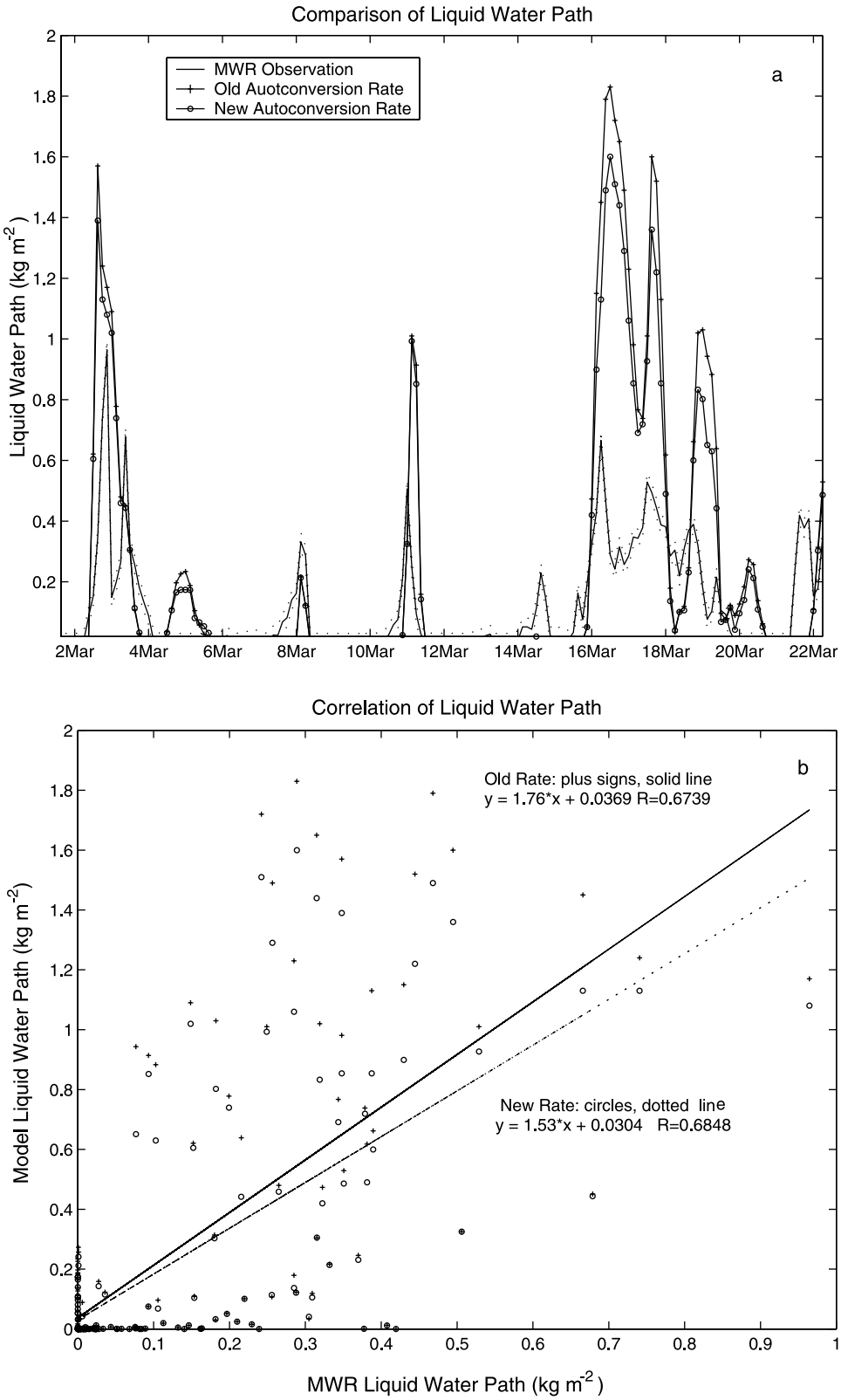

Figure 6. Comparison of liquid water path for ARM March 2000 IOP, a) comparison of liquid water path, the dotted line is the instantaneous uncertainty of the MWR LWP, b) correlation of MWR liquid water path versus model simulation, the solid line is the regression line of MWR LWP versus simulated LWP using the old autoconversion rate and the dotted line is the regression line of MWR LWP versus simulated LWP using the new autoconversion rate.

day^{-1}) around 3, 8, 16 and 17 March between 400 and 900 hPa. Around 11 and 19 March, there were two relatively weak cooling periods (about 25 K day^{-1}) between the same altitudes. The cold air advection is associated with moisture advection on 3, 8 and 16 March. Two extreme dry periods occur immediately before and after the 8 March moist period, maybe due to the wind direction change in this period. In the fall case, only one extreme large cooling period occurred on 23 September between 300 and 900 hPa, exceeding 50 K day^{-1}in the center of the cooling. The cold air tendency, as in the spring case, was also associated with a large moistening tendency in this area.

[24] The comparisons of liquid water path during the two IOPs are shown in Figures 6 and 7. The SCM captures the main tendency of liquid water path (LWP), but the model predicts larger liquid water paths than the observational data retrieved from microwave radiometer (MWR) measurement. The dotted line is the instantaneous uncertainty of the MWR observation mainly due to the retrieval method. The theoretical accuracy of the LWP measured by MWR is about ± 0.03 kg m^{-2} [*Liljegren*, 1994]. Using the original autoconversion rate, LWP sometimes exceeds the observational value by more than a factor of 2, for instance, during the period of 16 to 18 March in the spring 2000 IOP and the period of 23 to 24 September in the fall 1997 IOP. Although the simulated liquid water path using the new autoconversion rate is still larger than the observed value, it improves the model results, especially for high values of LWP. For these large LWP cases, the precipitation size drops generated in these clouds reach the surface (cf. Figures 8 and 9). In other words, considerable amounts of large water droplets (>300 μm) are formed, which would cause the microwave retrieval to underestimate LWP values due to neglecting scattering effects of large droplets. The scatter diagrams of observed LWP versus simulated LWP show that simulated values are well correlated with the observational data, the correlation coefficients are larger than 0.67. The slopes of the regression lines indicate that the simulated LWPs are larger than the observation data. Using the new autoconversion rate, the slope of the regression line is improved from 1.76 to 1.53 and from 1.86 to 1.69 for the spring case and the fall case, respectively.

[25] Figures 8 and 9 are the comparisons of precipitation. The observational data is from surface precipitation gauge measurements. Again, the model captures most of the precipitation events, especially for the fall case and the rainfall event around 3 March for the spring case. However, the SCM almost misses the rainfall event around 8 and 11 March for the spring case, and generally the simulated precipitation is less than observed. The slopes of the regression lines between the simulated and observed precipitation are about 0.5 and 0.7 for the spring and fall case, respectively. This is consistent with the results for liquid water path, that is too little precipitation indicates that more water content stays in the clouds. The change of the autoconversion rate only has a small influence on the maximum precipitation. However, if we examine the figure in detail, the autoconversion has an effect on the onset of precipitation. Such assuming a distribution of cloud water rather than a mean cloud water value speeds up precipitation formation in parts of the clouds that have high liquid water. As a result, the liquid water in the cloud decreases and subsequently the conversion from cloud water to rain decreases. That is, even the new autoconversion rate is larger than the old one, it has little influence on the precipitation at later stages. Moreover, there is no cloud water advection provided in the ARM data, lack of mesoscale moisture may prohibit the formation of cloud water. Also the subgrid variance of liquid water might be underestimated by equation (13) and the large-scale forcing could be sufficiently inaccurate to form precipitation may account for the underestimated precipitation in the SCM.

[26] The simulated precipitation correlates well with the surface observation for both parameterizations in both cases as shown in Figures 8b and 9b. The correlation coefficients are as high as 0.98 for the fall case, and slightly less than 0.8 for the spring case. The correlation for spring case is smaller mainly because two precipitation events are missed in the simulations as shown in Figure 8a. This also results in the flatter slopes for these regression lines. As the new autoconversion rate has little influence on the precipitation at later stages, the differences in correlation coefficients and slopes of regression lines between the new and original autoconversion rate are negligible in both cases.

[27] Figures 10 and 11 show the comparison of total cloud cover. Total cloud cover is observed by the GOES satellite [*Minnis et al.*, 1995; *Minnis and Smith*, 1998]. As for the precipitation, the change of the autoconversion rate has little influence on total cloud cover. The SCM performs reasonably well in simulating total cloud cover for both cases, although there are some differences. During the periods 4–6 March, and 20–21 March in the spring IOP, the SCM predicts larger cloud cover than observed. However, in fall IOP, the SCM predicts less total cloud cover. It almost fails to predict the clouds observed during 18–20 September, and after 26 September. Comparison of the simulated and observed relative humidity does not show significant differences between them. The disagreement in cloud cover may be due to the different spatial scales represented in the satellite observation and in the SCM simulations.

4.2. Simulation of the SHEBA Case

[28] The goal of SHEBA is to investigate the role of Arctic climate in global change. It mainly focuses on: 1. Determine the ocean–ice–atmosphere processes that control the surface albedo and cloud-radiation feedback mechanisms over the Arctic pack ice, and to use this information to demonstrably improve models of Arctic ocean–atmosphere–ice interactive processes, 2. Develop and implement models that improve the simulation of the present-day Arctic climate, including its variability into coupled global climate models [http://sheba.apl.washington.edu/about/about.html]. Due to the extreme conditions in Arctic area, it is very difficult to obtain the needed forcing data to drive SCM. In our case study, the SHEBA year is simulated by nudging temperature and specific humidity toward the reanalysis data of the European Center for Medium Range Weather Forecasts (ECMWF) (C. S. Bretherton et al., A comparison of the ECMWF forecast model with observations over the annual cycle at SHEBA, submitted to *Journal Geophysical Research*, 2001). The ECMWF data at each time step were taken from the grid box closest to the SHEBA ship.

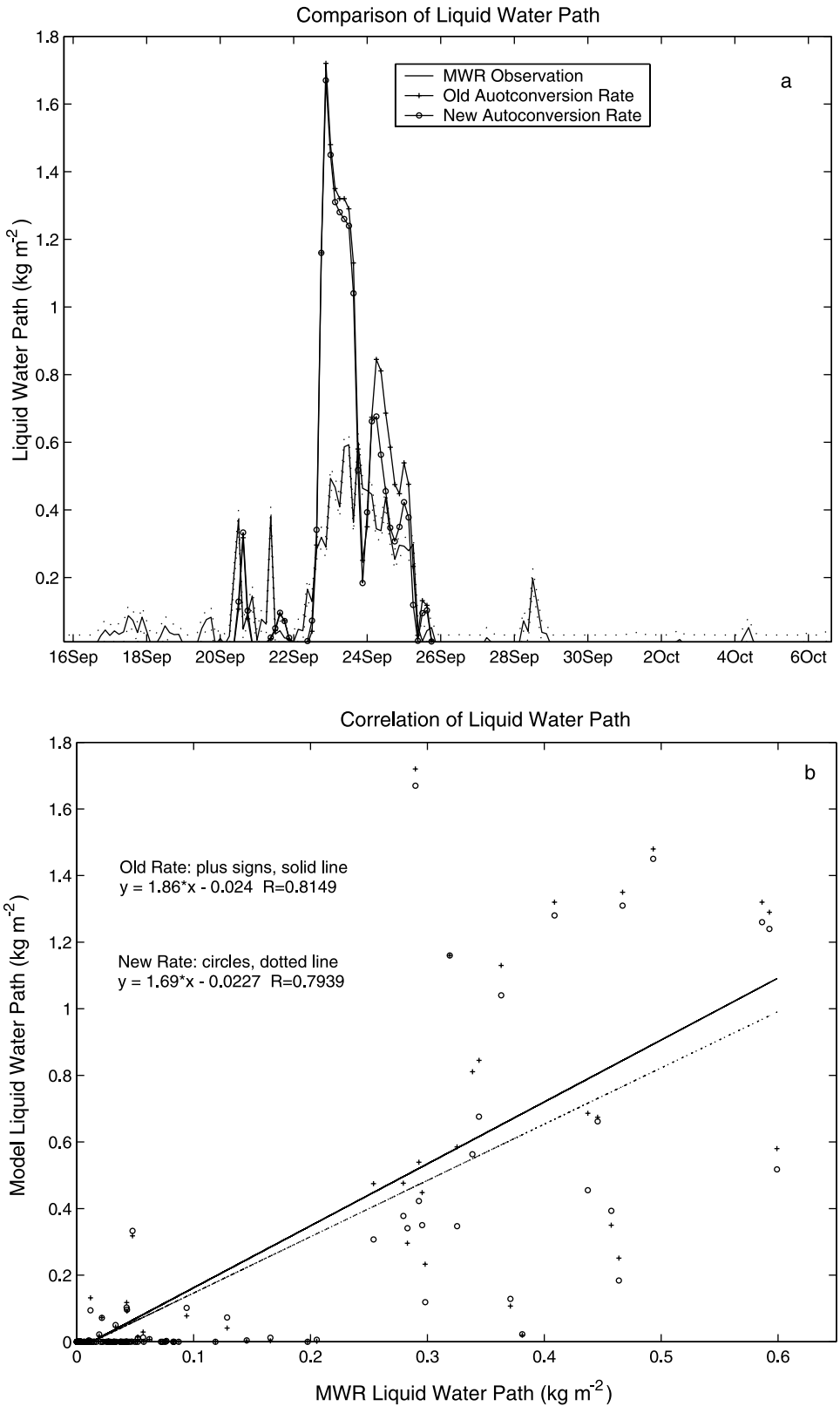

Figure 7. Same as Figure 6, but for ARM September 1997 IOP.

[29] The observational data used to verify the model simulation include LWP, precipitation and total cloud cover. As in the ARM case, the LWP values are retrieved from the MWR measurements. Because of the special Arctic environment, the LWP derived with the standard ARM retrieval algorithm has a large bias compared to the in situ aircraft observation. Comparisons between the in situ aircraft measurement taken in May–July 1998 show that the average

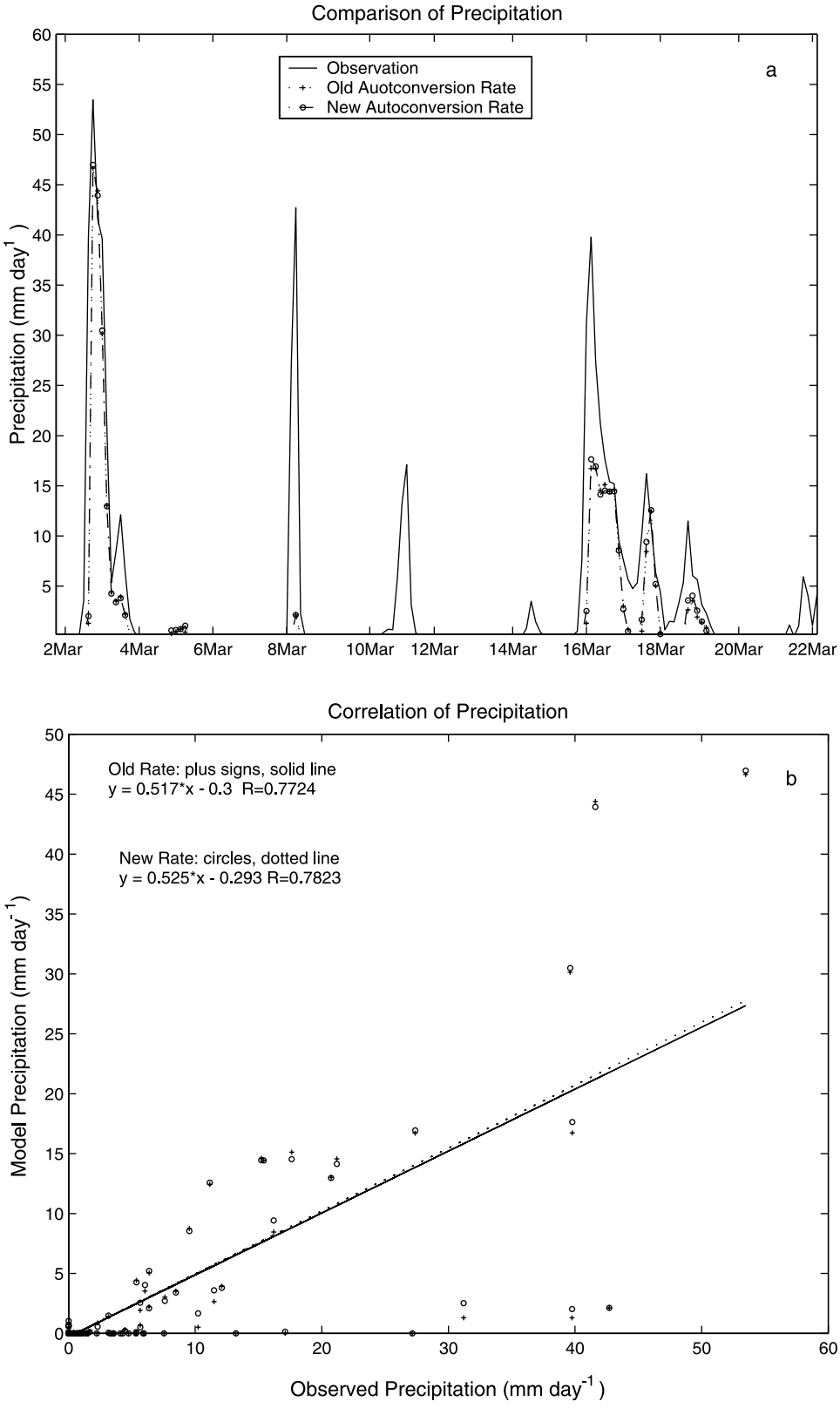

Figure 8. Same as Figure 6, but for precipitation in March 2000 IOP.

aircraft measurements are only half as large as the values derived from MWR using the standard retrieval method [*Lin et al.*, 2001]. In this paper, a new algorithm adopted from satellite remote sensing technique is used to retrieve LWP [*Lin et al.*, 2001]. Column water vapor (CWV) is estimated simultaneously with LWP as a by-product, due to dual channel characteristics of MWR. The mean LWP values obtained with this method only have a 3% difference with

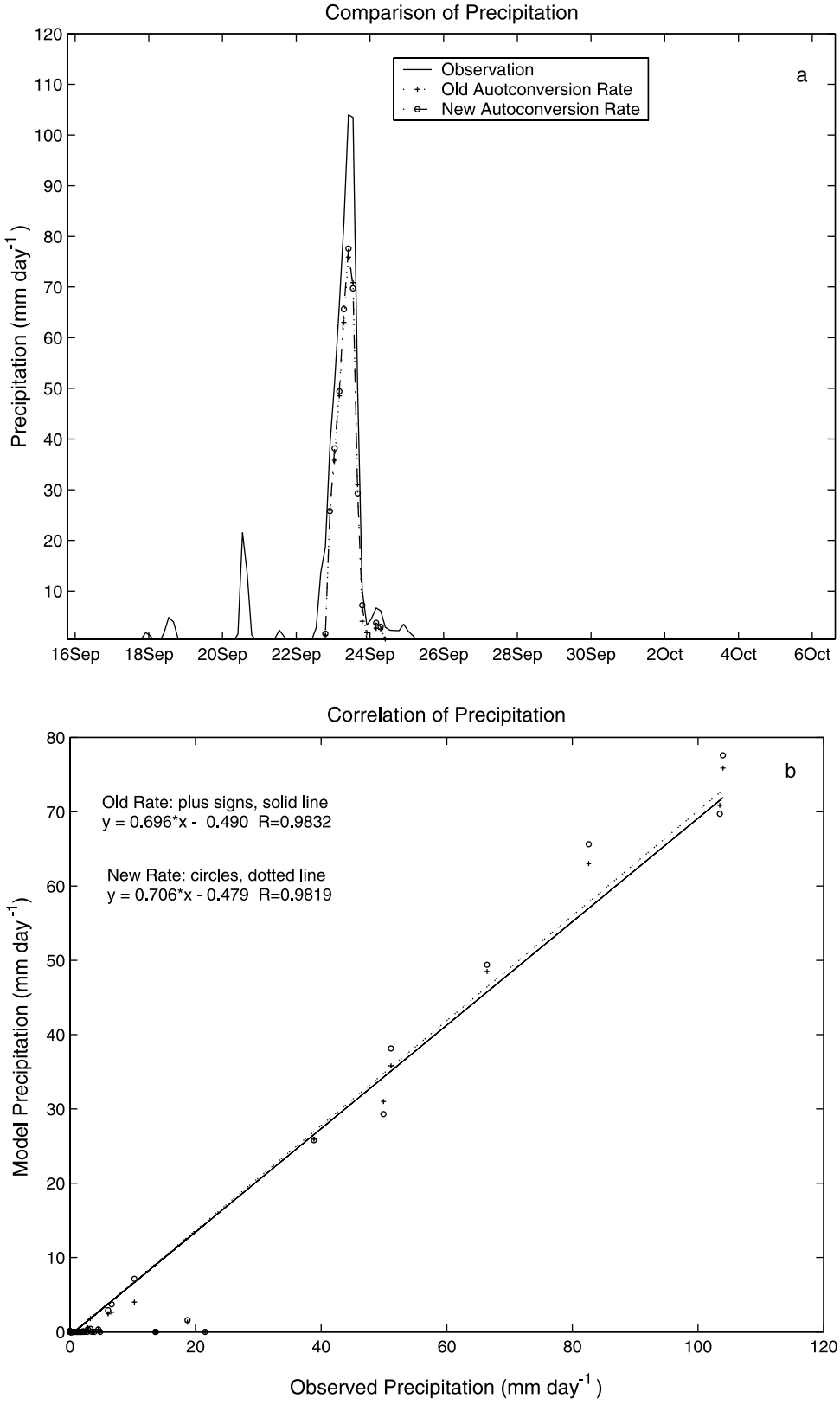

Figure 9. Same as Figure 6, but for precipitation in September 1997 IOP.

the more reliable in situ data. Precipitation data is from the SHEBA Project Office maintained Nipher shielded snow gauge system about 300 m from the SHEBA ship [*Persson et al.*, 2002]. Corrections were made for wind, losses due to evaporation and gauge wetting, and precipitation amount in intervals in which the reported weather is blowing (rather than falling) snow are set to zero. Cloud cover is from 8mm radar observation [*Intrieri et al.*, 2002].

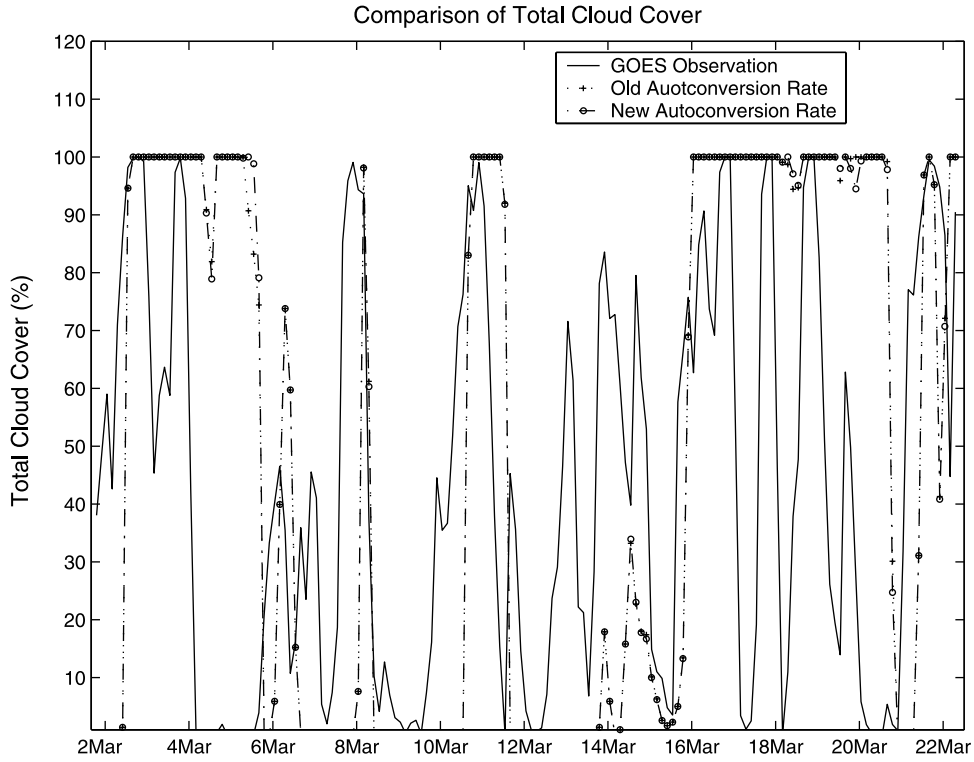

Figure 10. Comparison of total cloud cover for ARM March 2000 IOP.

[30] Figure 12 shows the monthly mean column water vapor (CWV) retrieved from MWR and average temperature predicted from ECMWF between the surface and 300 hPa level. The lowest average temperature occurs in December (about 240 K) and the highest temperature in July (about 260 K). The monthly mean CWV has a same tendency as temperature. In winter and spring it is very low, less than 5 kg m^{-2} from September to April. It increases

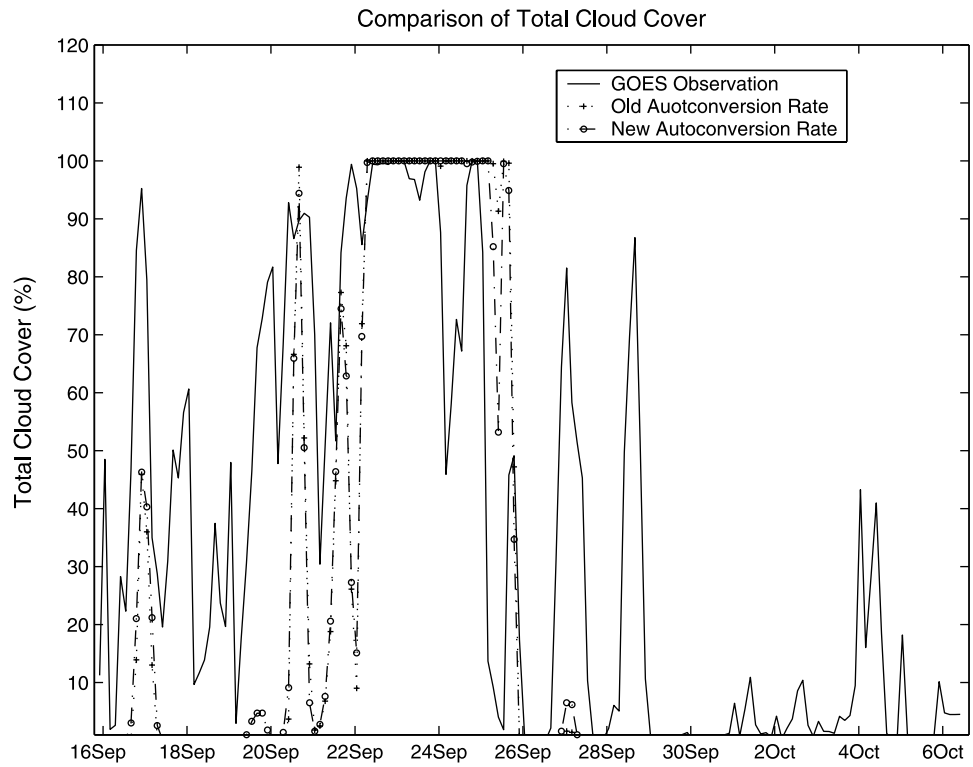

Figure 11. Comparison of total cloud cover for ARM September 1997 IOP.

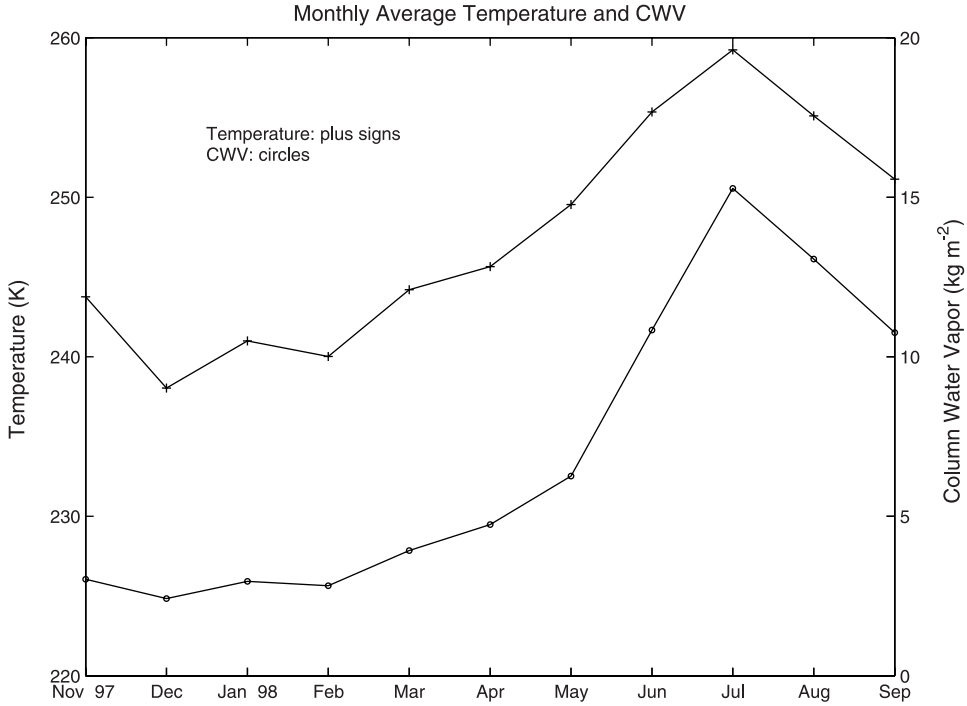

Figure 12. Monthly mean MWR observed Column Water Vapor (CWV) and average temperature predicted by ECMWF between the surface and 300 hPa level for the SHEBA year.

sharply from May to its maximum value in July. CWV exceeds 10 kg m^{-2} from June to September.

[31] Figure 13 shows the comparison of monthly averaged liquid water path, precipitation and total cloud cover for the period from November 1997 to September 1998. The dotted line in Figure 13a is the instantaneous uncertainty of the MWR retrieved liquid water path. As can be seen from Figure 13a that LWP closely follows the trend for CWV over the eleven-month period as shown in Figure 12. During the winter and spring months, from November to June, the new and old autoconversion rates of the SCM predict almost the same LWP, and they agree well with the

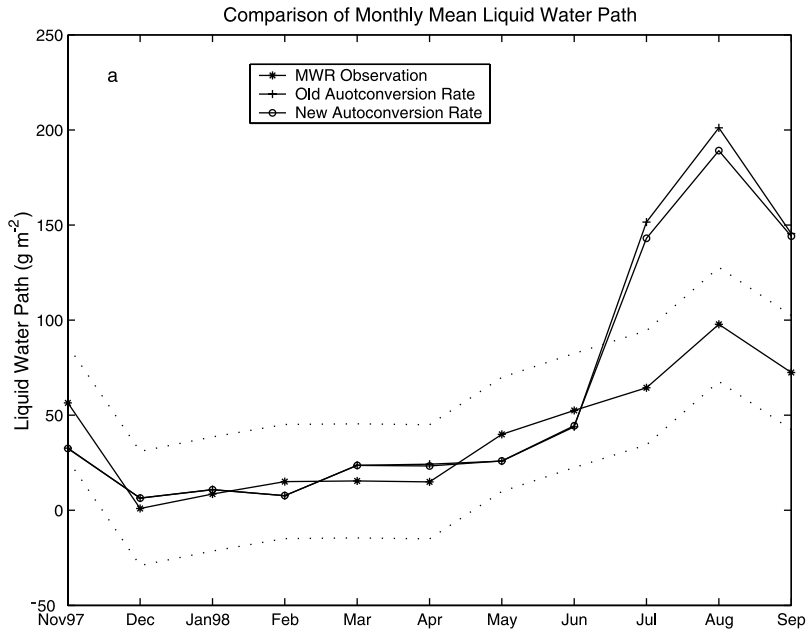

Figure 13. Comparison of monthly averaged liquid water path, precipitation and total cloud cover for the SHEBA year from November 1997 to September 1998, a) comparison of liquid water path, the dotted line is the instantaneous uncertainty of the MWR LWP, b) comparison of precipitation, and c) comparison of total cloud cover.

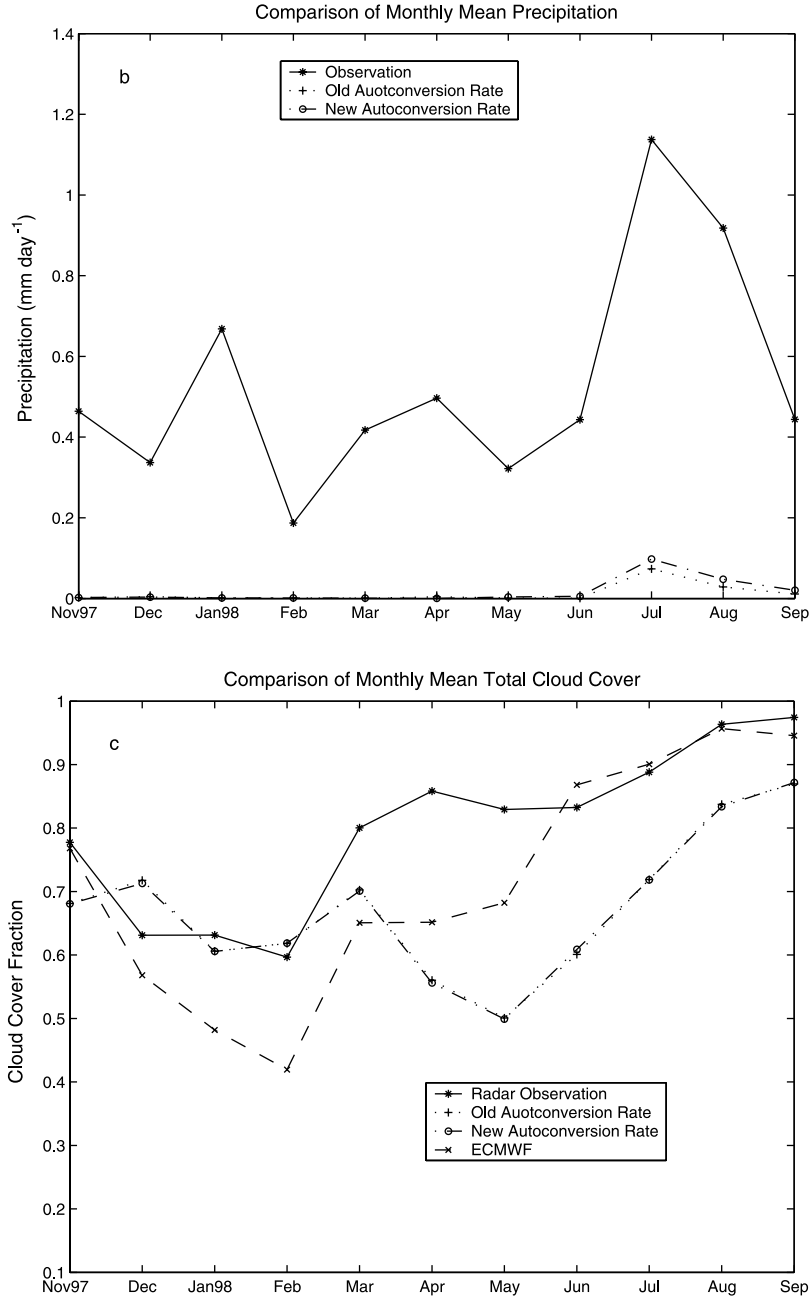

Figure 13. (continued)

MWR observations. However, in summer (July, August and September), when LWP is high, the LWP simulated by the SCM is larger than observed by MWR. Using the old autoconversion rate, the simulated LWP is about twice as high as the observed values, as was the case for the ARM IOPs. The new autoconversion rate reduces the LWP differences and improves the SCM simulation during this period, although it still over predicts LWP.

[32] Figure 13b shows that precipitation is drastically underpredicted during the whole SHEBA period. From November 1997 to June 1998, the SCM predicts nearly zero precipitation. In the other three months (July, August and September), the simulated precipitation follows the same trend as the observed values, but it is about an order of magnitude smaller than the observed. Considering that in the Arctic region even in the warmest month (July) the average temperature between the surface and 300 hPa is only about 260k (Figure 12), the precipitation mainly falls as snow, especially in the winter. For improving the prediction in this region, one needs to look into the precipitation formation via the ice phase. This is beyond the scope of this study but will be addressed in future. Although the SCM predicts much smaller precipitation rates than observed, the new parameterization still improves the model predictions in the warmer period from June to September.

[33] The simulated total cloud cover in Figure 13c follows the same trend as the radar observations and that predicted by ECMWF. However, large disagreements from the observations occur in spring (from April to June), where the model seriously underestimates cloud cover independent of the

autoconversion parameterizations used. It could be due to errors in the input data of temperature and humidity from the reanalysis data of ECMWF or the distribution function that is being used. This will be further investigated in future.

5. Summary and Conclusions

[34] In this paper, we discussed a new statistical based autoconversion rate originally derived from the stochastic collection equation. The in-cloud variability is included in this new parameterization by integrating the autoconversion rate over the cloudy part of the grid box. Because of the highly nonlinear dependence of the autoconversion rate on the liquid water content, the new rate is larger than the old one calculated from the mean liquid water content in the cloudy part. This is consistent with the need to artificially increase the original autoconversion rate in the ECHAM GCM as explained by *Lohmann and Roeckner* [1996]. Using the new autoconversion rate would thus reduce the enhancement of this process necessary in large scale models.

[35] Three cases have been used to test this new parameterization in different locations and seasons using the Canadian SCM. The results show that the new autoconversion rate improves the modeled liquid water path for all cases. Its impact on precipitation is minor. There is a slight improvement of precipitation for the summer time Arctic simulation, and a minor change in precipitation onset for the midlatitude cases. The influence of the change in autoconversion rate on the total cloud cover is negligible in all cases. Similar results also are achieved using a bounded triangle distribution function as used by *Smith* [1990] where an analytic expression of (18) can be obtained (not shown).

[36] Generally the model simulated liquid water path is still larger than the observed data when using the new autoconversion rate except for the winter and spring seasons in the Arctic where clouds mainly consist of ice crystals. Other nonlinear physical processes such as the aggregation rate of ice crystals to form snow flakes also need the same treatment to include the in-cloud variability in the parameterization. This will be addressed in future.

[37] **Acknowledgments.** This research is supported by the National Science and Research Council of Canada (NSERC), the Canadian foundation for Climate and Atmospheric Science and the National Science Foundation, and the NSF SHEBA project. Data for ARM cases were obtained from the Atmospheric Radiation Measurement (ARM) Program sponsored by the U.S. Department of Energy, Office of Science, Office of Biological and Environmental Research, Environmental Sciences Division. We thank Christian Jakob and his coworkers at ECMWF for producing the ECMWF column data set for SHEBA, Janet Intrieri and Taneil Uttal and their coworkers at NOAA/ETL for providing the radar and lidar data sets, Alice Fan for MWR data processing and Ed Andreas, Chris Fairall, Peter Guest, and Ola Persson in the SHEBA Atmospheric Surface Flux Group for help collecting and processing the data. We also thank Glen Lesins, Norman McFarlane, Knut Von Salzen and two anonymous reviewers for their comments on this paper.

References

Abdella, K., and N. McFarlane, A new second order turbulence closure scheme for the planetary boundary layer, *J. Atmos. Sci.*, *54*, 1850–1867, 1997.

Abdella, K., and N. McFarlane, Modelling boundary-layer clouds with a statistical cloud scheme and a second-order turbulence closure, *Boundary Layer Meteorol.*, *98*, 387–410, 2001.

Beheng, K. D., A parameterization of warm cloud microphysical conversion processes, *Atmos. Res.*, *33*, 193–206, 1994.

Boucher, O., H. Le Treut, and M. B. Baker, Precipitation and radiation modeling in a general circulation model: Introduction of cloud microphysical processes, *J. Geophys. Res.*, *100*, 16,395–16,414, 1995.

Collins, W. D., W. C. Conant, and V. Ramanathan, Earth radiation budget, cloud, and climate sensitivity, in *The Chemistry of the Atmosphere: Its Impact on Global Change*, edited by J. G. Calvert, pp. 207–215, Blackwell, Malden, Mass., 1994.

Fouquart, Y., and B. Bonnel, Computations of solar heating of the earth's atmosphere: A new parameterization, *Beitr. Phys. Atmos.*, *53*, 35–62, 1980.

Ghan, S., et al., A comparison of single column model simulations of summertime midlatitude continental convection, *J. Geophys. Res.*, *105*, 2091–2124, 2000.

Houghton, J. T., L. G. M. Filho, B. A. Callander, N. Harris, A. Kattenberg, and K. Maskell (Eds.), *Climate Change 1995*, *The Science of Climate Change: Intergovernmental Panel on Climate Change*, Cambridge Univ. Press, New York, 1996.

Intrieri, J. M., M. D. Shupe, T. Uttal, and B. J. McCarty, Annual cycle of Arctic cloud geometry and phase from radar and lidar at SHEBA, *J. Geophys. Res.*, *107*, 10.1029/2000JC000423, 2002.

Jiang, H., W. R. Cotton, J. O. Pinto, J. A. Curry, and M. J. Weissbluth, Cloud resolving simulations of mixed-phase Arctic stratus observed during BASE: Sensitivity to concentration of ice crystals and large-scale heat and moisture advection, *J. Atmos. Sc.*, *57*, 2105–2117, 2000.

Levkov, L., B. Rockel, H. Kapitza, and E. Raschke, 3D mesoscale numerical studies of cirrus and stratus clouds by their time and space evolution, *Beitr. Phys. Atmos.*, *65*, 35–58, 1992.

Liljegren, J. C., Two-channel microwave radiometer for observations of total column precipitable water vapor and cloud liquid water path, in *Fifth Symposium on Global Change Studies*, pp. 262–269, Am. Meteorol. Soc., Boston, Mass., 1994.

Lin, B., P. Minnis, A. Fan, J. A. Curry, and H. Gerber, Comparison of cloud liquid water paths derived from in situ and microwave radiometer data taken during the SHEBA/FIREACE, *Geophys. Res. Lett.*, *28*, 975–978, 2001.

Lohmann, U., and E. Roeckner, Design and performance of a new cloud microphysics scheme developed for the ECHAM general circulation model, *Clim. Dyn.*, *12*, 557–572, 1996.

Lohmann, U., N. McFarlane, L. Levkov, K. Abdella, and F. Albers, Comparing different cloud schemes of a single column model by using mesoscale forcing and nudging technique, *J. Clim.*, *12*, 438–461, 1999.

Lohmann, U., J. Humble, W. R. Leaitch, G. A. Isaac, and I. Gultepe, Simulations of ice clouds during FIRE ACE using the CCCMA single-column model, *J. Geophys. Res.*, *106*, 15,123–15,138, 2001.

Minnis, P., and W. L. Smith Jr., Cloud and radiative fields derived from GOES-8 during SUCCESS and the ARM-UAV Spring 1996 Flight Series, *Geophys. Res. Lett.*, *25*, 1113–1116, 1998.

Minnis, P., W. L. Smith Jr., D. P. Garber, J. K. Ayers, and D. R. Doelling, Cloud properties derived from GOES-7 for spring 994 ARM intensive observing period using version 1.0.0 of ARM satellite data analysis program, *NASA RP 1366*, 1995.

Morcrette, J. J., Radiation and cloud radiative properties in the European Centre for Medium Range Weather Forecasts forecasting system, *J. Geophys. Res.*, *96*, 9121–9132, 1991.

Persson, P. O. G., C. W. Fairall, E. L. Andreas, P. S. Guest, and D. K. Perovich, Measurements near the atmospheric surface flux group tower at SHEBA: Near-surface conditions and surface energy budget, *J. Geophys. Res.*, *107*(C10), 8045, doi:10.1029/2000JC000705, 2002.

Pincus, R., and S. A. Klein, Unresolved spatial variability and microphysical process rates in large-scale models, *J. Geophys. Res.*, *105*, 27,059–27,065, 2000.

Randall, D. A., K. M. Xu, R. J. Somerville, and S. Iacobellis, Single column models and cloud ensemble models as links between observations and climate models, *J. Clim.*, *9*, 1683–1697, 1996.

Richard, J. L., and J. F. Royer, A statistical cloud scheme for use in an AGCM, *Ann. Geophys.*, *11*, 1095–1115, 1993.

Rotstayn, L. D., A physically based scheme for the treatment of stratiform clouds and precipitation in large-scale models, 1, Description and evaluation of the microphysical processes, *Q. J. R. Meteorol. Soc.*, *123*, 1227–1282, 1997.

Rotstayn, L. D., A physically based scheme for the treatment of stratiform clouds and precipitation in large-scale models, 2, Comparison of modeled and observed climatological fields, *Q. J. R. Meteorol. Soc.*, *124*, 389–415, 1998.

Rotstayn, L. D., On the "tuning" of autoconversion parameterizations in climate models, *J. Geophys. Res.*, *105*, 15,495–15,507, 2000.

Smith, R. N., A scheme for predicting layer clouds and their water content in a general circulation model, *Q. J. R. Meteorol. Soc.*, *116*, 435–460, 1990.

Sommeria, G., and J. W. Deardorff, Subgrid-scale condensation in models of nonprecipitating clouds, *J. Atmos. Sci.*, *34*, 344–355, 1977.

Wilson, D. R., and S. P. Ballard, A microphysically based precipitation scheme for the UK Meteorological Office Unified Model, *Q. J. R. Meteorol. Soc.*, *125*, 1607–1636, 1999.

Xu, K. M., and D. A. Randall, Evaluation of statistically based cloudiness parameterizations used in climate models, *J. Atmos. Sci.*, *53*, 3103–3119, 1996.

Zhang, G. J., and N. A. McFarlane, Sensitivity of climate simulations to the parameterization of cumulus convection in the Canadian Climate Centre General Circulation Model, *Atmos. Ocean*, *33*, 407–446, 1995.

Zhang, M. H., and J. L. Lin, Constrained variational analysis of sounding data based on column-integrated budgets of mass, heat, moisture, and momentum: Approach and application to ARM measurements, *J. Atmos. Sci.*, *54*, 1503–1524, 1997.

Zhang, M. H., J. L. Lin, R. T. Cederwall, J. J. Yio, and S. C. Xie, Objective analysis of ARM IOP data: Method and sensitivity, *Mon. Weather Rev.*, *129*, 295–311, 2001.

B. Lin, NASA Langley Research Center, Hampton, VA 23681, USA.

U. Lohmann and J. Zhang, Department of Physics and Atmospheric Science, Dalhousie University, Halifax, Nova Scotia, Canada B3H 3J5. (zhang@mathstat.dal.ca)